

# NJC

Accepted Manuscript



This is an *Accepted Manuscript*, which has been through the Royal Society of Chemistry peer review process and has been accepted for publication.

*Accepted Manuscripts* are published online shortly after acceptance, before technical editing, formatting and proof reading. Using this free service, authors can make their results available to the community, in citable form, before we publish the edited article. We will replace this *Accepted Manuscript* with the edited and formatted *Advance Article* as soon as it is available.

You can find more information about *Accepted Manuscripts* in the [Information for Authors](#).

Please note that technical editing may introduce minor changes to the text and/or graphics, which may alter content. The journal's standard [Terms & Conditions](#) and the [Ethical guidelines](#) still apply. In no event shall the Royal Society of Chemistry be held responsible for any errors or omissions in this *Accepted Manuscript* or any consequences arising from the use of any information it contains.



## Crystal structure and luminescence properties of a novel $\text{Ce}^{3+}$ and $\text{Ce}^{3+}$ , $\text{Sm}^{3+}$ -activated $\text{Y}_4\text{SiAlO}_8\text{N}$ phosphors for near-UV white LEDs

Youjie Hua<sup>a, b</sup>, Xiaojun Li<sup>b</sup>, Dawei Zhang<sup>a\*</sup>, Hongping Ma<sup>c</sup>, Degang Deng<sup>b</sup>, Shiqing Xu<sup>b\*</sup>

Received 00th January 20xx,  
Accepted 00th January 20xx

DOI: 10.1039/x0xx00000x

www.rsc.org/

**Abstract:** A series of novel  $\text{Ce}^{3+}$  and/or  $\text{Sm}^{3+}$  activated  $\text{Y}_4\text{SiAlO}_8\text{N}$  (YSAON) phosphors are successfully synthesized by a conventional solid-state reaction method. The monophasic formation of YSAON is confirmed by X-ray powder diffraction (XRD) analysis. The crystal structure of YSAON is solved by XRD refinement data. The DFT calculation indicates that  $\text{Y}_4\text{SiAlO}_8\text{N}$  has an indirect band gap of 3.819 eV. Based on the analysis of crystal structure and lifetime curves, four emission sites of YSAON:  $0.02\text{Ce}^{3+}$  is determined as Y1 (413 nm, 448 nm), Y2 (428 nm, 469 nm), Y3 (619 nm, 698 nm) and Y4 (512 nm, 569 nm), respectively. The concentration quenching mechanism of  $\text{Ce}^{3+}$  in YSAON is discussed in detail and is confirmed as dipole–dipole interactions. Photoluminescence excitation (PLE) and Photoluminescence (PL) spectra measurements showed that the  $\text{Ce}^{3+}$  and  $\text{Sm}^{3+}$  co-doped phosphor could be efficiently excited by near-UV light, and exhibited four emission bands peaked at 485nm, 565nm, 605nm and 650 nm respectively. The CIE chromaticity of obtained white light can pass through by adjusting the content of  $\text{Ce}^{3+}$  and  $\text{Sm}^{3+}$  ions. Therefore, we anticipate that these materials can be used in near-UV chip pumped white LEDs.

**Key word:**  $\text{Y}_4\text{SiAlO}_8\text{N}$ ; Crystal structure; Luminescence; White LEDs

### 1 Introduction

In past decade, solid-state lighting has made tremendous progress and penetrated deeply into various market segments, such as automotive lighting, indoor and outdoor lighting, medical applications and also lifestyle products.<sup>1,2</sup> Compared with the previous incandescent and fluorescent lamps, the new solid-state lighting technique based on phosphor converted white-light emitting diodes (pc-WLEDs) shows many advantages, such as long lifetime, small volume, toxicity-free and environmentally friendly characteristics.<sup>3</sup> Most commercially available pc-WLEDs are based on blue-LED chips combined with YAG:  $\text{Ce}^{3+}$  as a yellow-emitting phosphor material.<sup>4,5</sup> However, the obvious drawbacks of this combination are low color-rendering index (CRI) and high color temperature due to the limited spectral power distribution in the red spectral range.<sup>6,7</sup> Consequently, an alternative approach that using near-UV (380 ~ 420 nm) LED chips coupled with red, green, and blue phosphors have been developed rapidly during the past few years.<sup>8</sup> This style can provide superior color uniformity with a high color rendering index and excellent quality of light. In both methods the conversion phosphors are playing an important role. Hence, it is

urgent to explore and develop new near-UV excitable phosphors to fulfill the requirements in the pc-WLEDs technology.

Compared with oxosilicates, the nitridosilicates and oxonitridosilicates are more appropriate host lattices for phosphors due to several advantages, such as high chemical stability, good thermal quenching ability, and exhibit intense luminescence for application in white LEDs.<sup>9,10</sup> However, the preparations of nitridosilicates always require critical synthesis conditions, such as high temperature and high pressure.<sup>9,10</sup> Accordingly, the oxonitridosilicates phosphors have attracted much more attention of people. Yttrium oxide and alumina are most frequently used as additives to promote sintering in silicon nitride and sialon ceramics.<sup>11,12</sup> A large amount of research has focused on Y–Si–O–N quaternary system applied for pc-WLEDs, such as  $\text{YSiO}_2\text{N}$ ,<sup>13</sup>  $\text{Y}_2\text{Si}_3\text{O}_7\text{N}_4$ ,<sup>14</sup>  $\text{Y}_4\text{Si}_2\text{O}_7\text{N}_2$ ,<sup>15-17</sup>  $\text{Y}_5\text{Si}_3\text{O}_{12}\text{N}$ ,<sup>18</sup>  $\text{Y}_6\text{Si}_3\text{O}_9\text{N}_4$ ,<sup>19</sup> and  $\text{Y}_{10}(\text{Si}_6\text{O}_{22}\text{N}_2)\text{O}_2$ .<sup>20</sup> Nevertheless, owing to critical preparation conditions, only a few papers have reported the luminescent properties of Y–Si–Al–O–N five component compounds. K. Liddell *et al* have studied X-Ray data for Y–Si–Al–O–N glass ceramics in detail but not for luminescent properties.<sup>21</sup> Wei-Ren Liu *et al* reported  $(\text{Ba}, \text{Sr})\text{Y}_2\text{Si}_2\text{Al}_2\text{O}_7\text{N}_5: \text{Eu}^{2+}$  as a novel near-ultraviolet converting green phosphor.<sup>22</sup> Woon Bae Park *et al* reported  $\text{Y}_{6+x/3}\text{Si}_{11-y}\text{Al}_y\text{N}_{20+x-y}\text{O}_{1-x+y}: \text{Re}^{3+}$  ( $\text{Re} = \text{Ce}^{3+}, \text{Tb}^{3+}, \text{Sm}^{3+}$ ) as a new oxynitride phosphor for use in white light-emitting diodes.<sup>23</sup> Wu and Xia *et al* studied the crystal structure and luminescence properties of  $\text{Y}_4\text{Si}_2\text{O}_7\text{N}_2: \text{Re}^{3+}$  ( $\text{Re} = \text{Ce}^{3+}, \text{Tb}^{3+}$ ) phosphors.<sup>16,17</sup>

In this paper, we prepared a series of novel  $\text{Ce}^{3+}$  and/or  $\text{Sm}^{3+}$  activated  $\text{Y}_4\text{SiAlO}_8\text{N}$  phosphors by a conventional solid-state reaction. The  $\text{Ce}^{3+}$  and  $\text{Sm}^{3+}$  co-activated phosphors can give

<sup>a</sup> School of Optical-Electrical and Computer Engineering, University of Shanghai for Science and Technology, Shanghai 200093, China

<sup>b</sup> College of Materials Science and Engineering, China Jiliang University, Hangzhou 310018, China. Fax: +86-571-28889527; Tel: +86-571-86835781; E-mail: sxucjlu@163.com

<sup>c</sup> School of Mechanical & Automotive Engineering, Zhejiang University of Science and Technology, Hangzhou 310012, China

excellent white-light emission directly in a single host. The crystal structure and luminescence properties of the  $Y_4SiAlO_8N: Ce^{3+}, Sm^{3+}$  phosphor has been investigated in detail.

## 2 Experimental

### 2.1 Sample preparation

A series of  $Ce^{3+}$  and/or  $Sm^{3+}$  activated  $Y_4SiAlO_8N$  phosphors were prepared by a high temperature solid-state reaction method.  $Y_2O_3$  (99.99%),  $SiO_2$  (99.99%),  $Al_2O_3$  (99.99%),  $\alpha-Si_3N_4$  (99.9%),  $CeO_2$  (99.995%) and  $Sm_2O_3$  (99.995%) were used as starting materials. They were weighed in stoichiometric proportions and mixed in an agate mortar. Then the mixture were placed into alumina crucible and sintered at 1500 °C for 6 hours under a reducing atmosphere (5% $H_2$  / 95% $N_2$  mixture). The products were then obtained by cooling down to room temperature in the furnace, grinding, and pulverizing for further measurements.

### 2.2 Characterization

The phase purity of obtained samples were checked by X-ray powder diffraction (XRD) analysis using a Bruker AXS D8 advance powder diffractometer, with  $CuK\alpha$  radiation operated at 40kV and 40mA. The  $2\theta$  ranges of all data sets were from 10° to 80° with a step size of 0.02° and a counting time of 5 seconds/step. The crystallographic data including lattice parameters, unit cell volume, and atomic positions were estimated by Rietveld refinement on the basis of the XRD data, using the  $Y_4Si_2O_7N_2$  (ICSD: 81860) as starting model.

The band structure and density of states (DOS) were calculated by density functional theory (DFT) method with the Cambridge Serial Total Energy Package (CASTEP) code.<sup>24-26</sup> For the calculations, the energy cut-off of the plane wave basis set was selected as 750 eV and K-point sampling was chosen as the  $2 \times 1 \times 1$ . Criterion for the self-consistent field (SCF) was eigen-energy convergence within  $3.468 \times 10^{-7}$  eV/atom.

The scanning electron microscopy (SEM) micrographs were obtained by using a SU8010 field-emission scanning electron microscope (Hitachi, Japan). The photoluminescence (PL) and photoluminescence excitation (PLE) spectra were measured at room temperature by FL3-211-P spectrofluorometer (Horiba Jobin Yvon, USA) equipped with a 450W Xe light source. The PL decay-curves were measured on the same spectrophotometer, which was combined with a Time-Correlated Single-Photon Counting (TCSPC) system. The diffuse reflectance spectra of these samples were measured by an ultraviolet-visible-near infrared spectrophotometer (UV3600) using  $BaSO_4$  as a reference in the range of 200–800 nm. All the above measurements were performed at room temperature.

## 3 Results and discussion,

### 3.1 Crystal structure of $Y_4SiAlO_8N$ host material

The host material of  $Y_4SiAlO_8N$  phosphor has been prepared successfully by a high temperature solid-state reaction method. Fig. 1 shows the experimental (black line) and calculated (red line) XRD

patterns for the Rietveld refinement result of  $Y_4SiAlO_8N$  host at room temperature. Due to the substitution of  $Al^{3+}$  and  $O^{2-}$ , the XRD diffraction peaks of  $Y_4SiAlO_8N$  and  $Y_4Si_2O_7N_2$  show obvious differences according the JCPDS (No. 48-1630) and JCPDS (No. 32-1451). However, according to the design principle of Chemical Unit Cosubstitution,<sup>27-28</sup> the crystal structure of  $Y_4SiAlO_8N$  can be regarded as isotypic to that of  $Y_4Si_2O_7N_2$  (ICSD: 81860) with a cosubstitution via the [Al-O] for [Si-N]. Thus the crystal structure of  $Y_4SiAlO_8N$  can be solved successfully by the Rietveld refinement on the basis of the XRD data using the  $Y_4Si_2O_7N_2$  (ICSD: 81860) as starting model. The results of Rietveld refinement indicate that a pure  $Y_4SiAlO_8N$  phase was formed without any impurities.

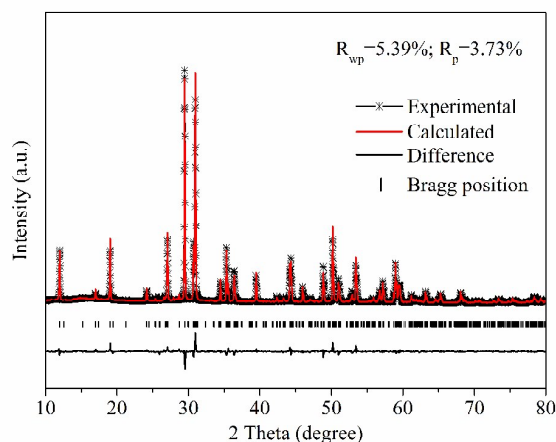


Fig. 1 Experimental and calculated XRD patterns of  $Y_4SiAlO_8N$ .

The crystallographic data of  $Y_4SiAlO_8N$  derived from Rietveld refinement of X-ray diffraction are presented in Table 1. The crystal structure of  $Y_4SiAlO_8N$  was solved and refined as monoclinic system and space group  $P121/c1$  (14) with  $a=7.4491\text{Å}$ ,  $b=10.3933\text{Å}$ ,  $c=11.0563\text{Å}$ ,  $\beta=109.7109^\circ$ . The refinement finally converged to satisfy the reflection condition well with the residual factors to  $R_{wp} = 5.39\%$ ,  $R_p = 3.73\%$  and goodness of fit (GOF) = 1.52. The atomic coordinates, isotropic displacement parameters, and site occupancies of  $Y_4SiAlO_8N$  host are presented in Table 2. There are obvious differences of the atomic positions and cell volume between  $Y_4SiAlO_8N$  and  $Y_4Si_2O_7N_2$  according to ref.11.

Table 1 Crystallographic data of  $Y_4SiAlO_8N$  derived from Rietveld refinement of X-ray Diffraction.

Space group:	$Pmnb: ba-c$ (orthorhombic)
Formula	$Y_4SiAlO_8N$
Crystal system	monoclinic
Space group	$P 1 21/c 1$ (14)
Lattice parameters (Å, °)	$a=7.4491\text{Å}$ , $b=10.3933\text{Å}$ , $c=11.0563\text{Å}$ , $\beta=109.7109^\circ$
Cell volume (Å <sup>3</sup> )	805.83 Å <sup>3</sup>
Formula units per unit cell, Z	4
Calculated density	4.55536 g/cm <sup>3</sup>
Temperature (K)	300 K

Radiation (Å)	Cu-Kα1 ( $\lambda = 1.54056 \text{ \AA}$ )
Profile range	$10.0 \leq \theta \leq 80.0$
R values	$R_{wp} = 5.39\%$ , $R_p = 3.73\%$
Goodness of fit, GOF	1.52

**Table 2** Atomic coordinates, isotropic displacement parameters, and site occupancies for  $Y_4SiAlO_8N$  determined by Rietveld Refinement of X-ray Diffraction.

Atom	Wycko ff Site	x	y	z	Occ	$U_{eq}/\text{\AA}^2$
Y1	4e	0.8373	0.12159	0.42661	1	0
Y2	4e	0.35224	0.12567	0.42558	1	0
Y3	4e	0.52818	0.40683	0.29812	1	0.0037
Y4	4e	0.02159	0.40185	0.29919	1	0.0095
Al	4e	0.7444	0.18886	0.12541	1	0
Si	4e	0.15698	0.18585	0.11227	1	0
N1	4e	0.95101	0.2411	0.10216	1	0
O1	4e	0.72617	0.03516	0.16247	1	0
O2	4e	0.21269	0.03114	0.16266	1	0
O3	4e	0.72414	0.27626	0.24133	1	0.0343
O4	4e	0.28561	0.26622	0.23633	1	0
O5	4e	0.58438	0.23407	-0.01508	1	0.0996
O6	4e	0.1661	0.22101	-0.026	1	0.001
O7	4e	0.43651	0.49627	0.10235	1	0
O8	4e	0.92974	0.52139	0.09057	1	0

The crystal structure of YSAON is shown in Fig. 2. Fig. 2 (a) shows a unit cell of the YSAON view toward the [111] axis. The structure of YSAON has four formula units in a unit cell, i.e. the unit cell contains  $16Y + 4Si + 4Al + 32O + 4N$  atoms. The YSAON structural type is characterized by [111] axis of Y coordination polyhedral sharing faces, which are linked with eight symmetric  $SiO_3N$  and  $AlO_3N$  tetrahedron forming a three-dimensional framework of polyhedral, as shown in Fig. 2 (a). Fig. 2 (b) shows coordination spheres and bond lengths of Y1, Y2, Y3 and Y4 sites. The YSAON has four  $Y^{3+}$  sites: Y1 is seven-coordinated with O and one-coordinated with N (coordination number CN=8); Y2 is seven-coordinated with O (CN=7); Y3 is six-coordinated with O (CN=6); Y4 is six-coordinated with O and one-coordinated with N (CN=7). Accordingly, different emission centers originated from the different sites will be discussed in detail below.

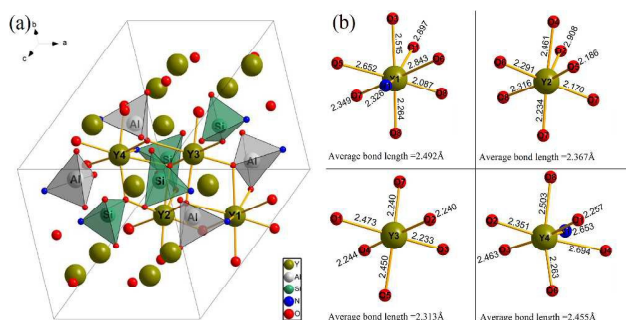


**Fig. 2** (a) Extended coordination spheres of Y, Si and Al in signal  $Y_4SiAlO_8N$  unit cell view toward the [111] axis; (b) Coordination spheres of Y1, Y2, Y3 and Y4 sites of  $Y_4SiAlO_8N$ .

### 3.2 Band structure of $Y_4SiAlO_8N$

Fig. 3 presents the calculated band structure of  $Y_4SiAlO_8N$  based on density functional theory (DFT) methods.<sup>24-26</sup> Here, the ground state GGA-PBE calculation was used for determining the band structure. The results indicate that the material has an indirect band gap of 3.819 eV, with the valence band (VB) maximum at B point and the conduction band (CB) minimum at G point. This broad band gap can provide an appropriate environment for the  $Ce^{3+}$  and  $Sm^{3+}$  emission.

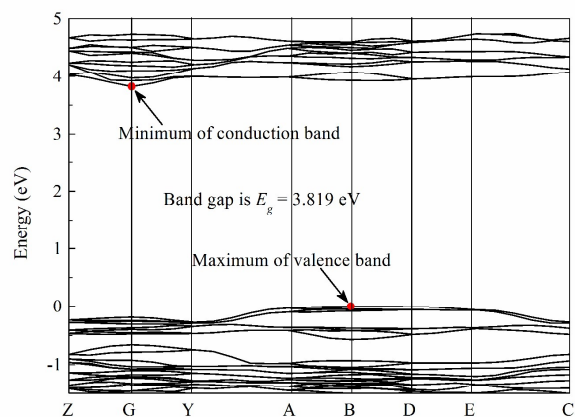


**Fig. 3** The band structure of  $Y_4SiAlO_8N$  based on density functional theory (DFT).

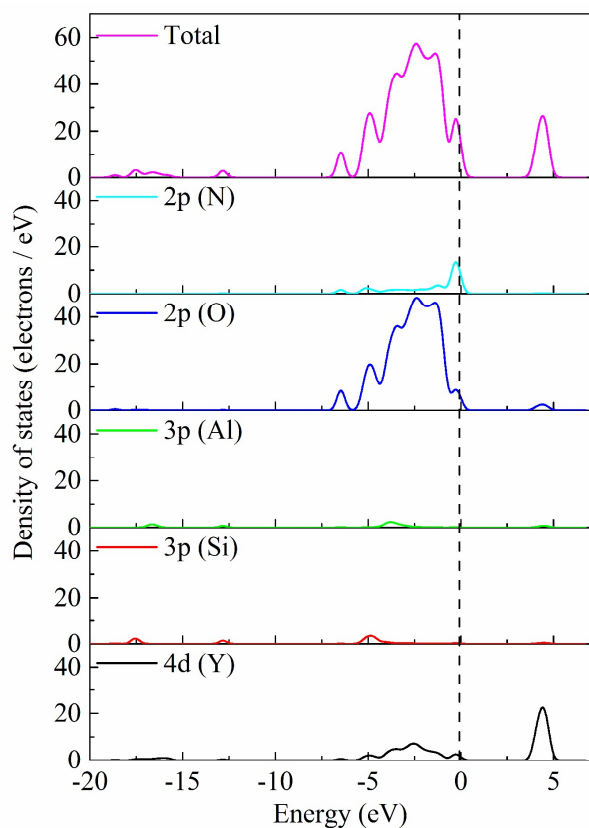


Fig. 4 Total and partial density of states of  $Y_4SiAlO_8N$ .

Fig. 3 presents the calculated band structure of  $Y_4SiAlO_8N$  based on density functional theory (DFT) methods.<sup>24-26</sup> Here, the ground state GGA-PBE calculation was used for determining the band structure. The results indicate that the material has an indirect band gap of 3.819 eV, with the valence band (VB) maximum at B point and the conduction band (CB) minimum at G point. This broad band gap can provide an appropriate environment for the  $Ce^{3+}$  and  $Sm^{3+}$  emission.

Fig. 4 shows the total and partial density of states (DOS) of  $Y_4SiAlO_8N$ , as determined by the ground state GGA-PBE calculation. It can be seen that the conduction band is mainly composed by dominant 4d (Y) orbitals and minor 2p (O) orbitals. The variations in the 4d (Y) orbitals are mirrored in the 2p (O) orbitals. This suggests covalent bonding within Y and O atoms. In the valence band, it is mainly composed by dominant 2p (O) orbitals and minor 4d (Y) orbitals, and some 2p (N) orbitals in the higher valence band. The 2p orbitals of N atoms have more contributions than that of O atoms to the top of the valence band; thus, it is deduced that nitrogen benefits reduction of the band gap for  $Y_4SiAlO_8N$ .<sup>29</sup> In addition, the coincident peaks are also been observed obviously between 2p (O) and 4d (Y) orbitals in the large range of lower valence band, implying this region is characterized by Y–O covalent bonds. Besides, the DOS variation of 2p (N) orbitals is coincident with 4d (Y) orbitals in the top of valence band. This also indicates that the Y atoms are coordinate with N atoms by

covalent bond. However, the bond energy of Y–N bond is less than that of Y–O bond.

### 3.3 Crystalline phases of $Y_4SiAlO_8N$ : $Ce^{3+}$ , $Sm^{3+}$ phosphors

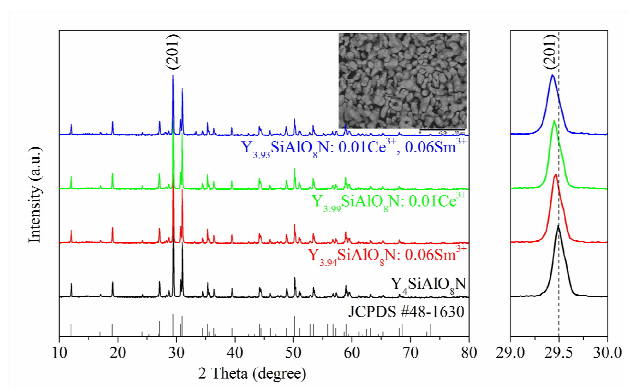
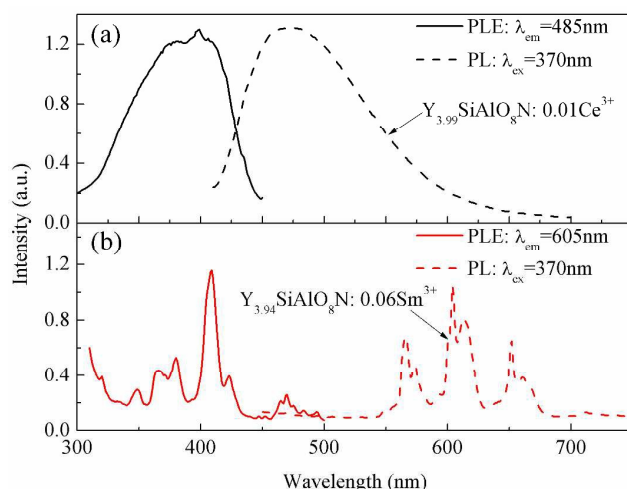


Fig. 5 The X-ray diffraction patterns of YSAON host, YSAON: 0.06 $Sm^{3+}$ , YSAON: 0.01 $Ce^{3+}$  and YSAON: 0.01 $Ce^{3+}$ , 0.06 $Sm^{3+}$  phosphors.

Fig. 5 shows the X-ray diffraction patterns of YSAON host, YSAON: 0.06 $Sm^{3+}$ , YSAON: 0.01 $Ce^{3+}$  and YSAON: 0.01 $Ce^{3+}$ , 0.06 $Sm^{3+}$  phosphors. It shows that all of the observed XRD peaks match well with the standard  $Y_4SiAlO_8N$  phase (JCPDS #48-1630). These results indicate that the monophasic  $Y_4SiAlO_8N$ -based phosphors have been synthesized and the crystalline phases could not be changed by doping  $Ce^{3+}$  and  $Sm^{3+}$  ions. However, the diffraction peaks of the YSAON: 0.06 $Sm^{3+}$ , YSAON: 0.01 $Ce^{3+}$  and YSAON: 0.01 $Ce^{3+}$ , 0.06 $Sm^{3+}$  samples shift slightly to a lower diffraction degree in contrast with that of the YSAON host. This is because the relationship of the ionic radii of  $Y^{3+}$ ,  $Ce^{3+}$  and  $Sm^{3+}$  is  $R_{Ce^{3+}} > R_{Sm^{3+}} > R_{Y^{3+}}$  in the YSAON host lattice. The above results indicate that  $Ce^{3+}$  and/or  $Sm^{3+}$  have been successfully introduced into the  $Y_4SiAlO_8N$  host lattice. In addition, the inset in Fig. 5 shows a typical scanning electron microscopy (SEM) image of as-prepared  $Y_4SiAlO_8N$ : 0.01 $Ce^{3+}$ , 0.06 $Sm^{3+}$  phosphor. The obtained powder consists of nearly spherical and well-dispersed particles with a diameter size range from 8 $\mu m$  to 10 $\mu m$  which is suitable for use in white LED packaging.

### 3.4 Photoluminescence of $Y_{4-x}SiAlO_8N$ : $xCe^{3+}$ phosphors



**Fig. 6** PLE and PL spectra of (a)  $\text{Y}_{3.99}\text{SiAlO}_8\text{N}: 0.01\text{Ce}^{3+}$  and (b)  $\text{Y}_{3.94}\text{SiAlO}_8\text{N}: 0.06\text{Sm}^{3+}$  phosphors.

Fig. 6(a) shows the excitation and emission spectra of  $\text{Y}_{3.99}\text{SiAlO}_8\text{N}: 0.01\text{Ce}^{3+}$  phosphor. Upon 370 nm near-UV light excitation, the PL spectra of YSAON:  $0.01\text{Ce}^{3+}$  phosphor shows an asymmetric emission band range from 420 nm to 600 nm due to the  $5d^1 \rightarrow 4f^1$  transition of  $\text{Ce}^{3+}$ . The broad emission band was attributed to the high covalency of the Ce–N bond and a large crystal-field splitting effect.<sup>17</sup> The excitation spectra of the YSAON:  $0.01\text{Ce}^{3+}$  phosphor monitored at 485 nm consist of a broad band in the region from 320 to 430 nm corresponding to the transition from  $4f^1$  ground state to  $5d^1$  excitation state of  $\text{Ce}^{3+}$  ions. Fig. 6(b) shows the excitation and emission spectra of  $\text{Y}_{3.94}\text{SiAlO}_8\text{N}: 0.06\text{Sm}^{3+}$  phosphor. It can be observed that the excitation spectrum includes a very strong band centered at 410 nm and several weak bands centered at 350 nm, 365 nm, 380 nm, 423 nm and 470 nm respectively. These excitation bands can be attributed to the  $^6\text{H}_{5/2} \rightarrow ^3\text{H}_{7/2}$  (350 nm),  $^6\text{H}_{5/2} \rightarrow ^4\text{L}_{17/2}$  (365 nm),  $^6\text{H}_{5/2} \rightarrow ^4\text{K}_{13/2}$  (380 nm),  $^6\text{H}_{5/2} \rightarrow ^4\text{F}_{7/2}$  (410 nm),  $^6\text{H}_{5/2} \rightarrow ^6\text{P}_{5/2}$  (423 nm) and  $^6\text{H}_{5/2} \rightarrow ^4\text{I}_{11/2}$  (470 nm) of  $\text{Sm}^{3+}$  ions, respectively.<sup>30</sup> Under 370 nm near-UV light excitation, the  $\text{Y}_4\text{SiAlO}_8\text{N}: \text{Sm}^{3+}$  phosphor shows three broad emission bands centered at 565 nm, 605 nm and 650 nm, which can be ascribed to the  $^4\text{G}_{5/3} \rightarrow ^6\text{H}_{5/2}$ ,  $^4\text{G}_{5/2} \rightarrow ^6\text{H}_{7/2}$  and  $^4\text{G}_{5/2} \rightarrow ^6\text{H}_{9/2}$  transitions of  $\text{Sm}^{3+}$  ions.<sup>31</sup> It suggests that both  $\text{Y}_4\text{SiAlO}_8\text{N}: \text{Ce}^{3+}$  and  $\text{Y}_4\text{SiAlO}_8\text{N}: \text{Sm}^{3+}$  phosphors can be excited effectively by near-UV LED chips. Consequently, under near-UV light excitation, we can obtain white light by co-doping  $\text{Ce}^{3+}$  and  $\text{Sm}^{3+}$  ions into  $\text{Y}_4\text{SiAlO}_8\text{N}$  host lattice due to their distinctive emission bands in visible light range. The Commission International de l'Eclairage (CIE) chromaticity coordinates; color-rendering index (CRI) and color temperature can be tuned by adjusting the content of  $\text{Ce}^{3+}$  and  $\text{Sm}^{3+}$  ions.

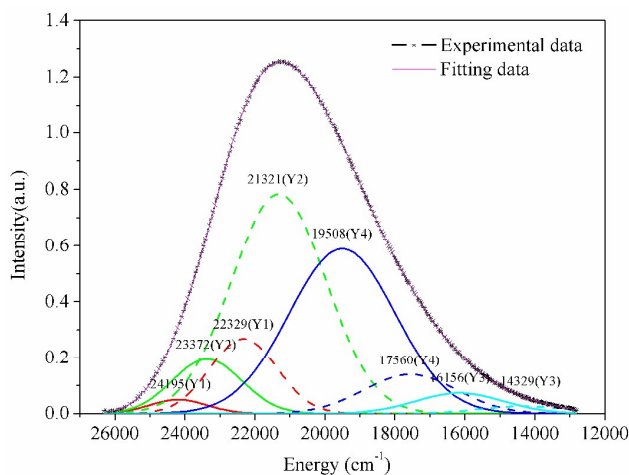


**Fig. 7** Gaussian fitting of the emission band of  $\text{Y}_{3.99}\text{SiAlO}_8\text{N}: 0.01\text{Ce}^{3+}$  phosphor.

The emission band of  $\text{Y}_{3.99}\text{SiAlO}_8\text{N}: 0.01\text{Ce}^{3+}$  was decomposed into eight well-separated Gaussian components, as shown in Fig. 7. It can be observed that this emission band center at: Y1:  $24195\text{ cm}^{-1}$  (413 nm),  $22329\text{ cm}^{-1}$  (448 nm); Y2:  $23372\text{ cm}^{-1}$  (428 nm),  $21321\text{ cm}^{-1}$  (469 nm); Y4:  $19508\text{ cm}^{-1}$  (512 nm),  $17560\text{ cm}^{-1}$  (569 nm); Y3:  $16156\text{ cm}^{-1}$  (619 nm),  $14329\text{ cm}^{-1}$  (698 nm). These distributed emission bands in different sites above can be explained as follow. At a same site,  $\text{Ce}^{3+}$  have two distinct emission bands with the theoretical energy value of  $2000\text{ cm}^{-1}$  because the emission of  $\text{Ce}^{3+}$  is attributed to transitions from two lowest 5d excited states ( $^2\text{D}_{3/2}$ ,  $^2\text{D}_{5/2}$ ) to two 4f ground states ( $^2\text{F}_{5/2}$ ,  $^2\text{F}_{7/2}$ ).<sup>32, 33</sup>

The emission site is closely related to the crystal field strength, which is influenced by site symmetry, covalency, ligand charge and bond length.<sup>32</sup> According to Uitert's report, the relationship between energetic position of  $\text{Ce}^{3+}$  emission and its local structure environment is suggested to obey an empirical equation<sup>34</sup>:

$$E = Q \times \left[ 1 - \left( \frac{V}{4} \right)^{\frac{1}{V}} 10^{\frac{n \times E_a \times r}{80}} \right] \quad (1)$$

where E is the position for the  $\text{Ce}^{3+}$  emission peak, Q is the position in energy for the lower d-band edge for the free  $\text{Ce}^{3+}$  ion, V is the valence of the  $\text{Ce}^{3+}$ , n is the coordination number (CN) of anions,  $E_a$  is the electron affinity of the atoms that form anions (eV), and r ( $\text{\AA}$ ) is the radius of the host cation replaced by the  $\text{Ce}^{3+}$ . For YSAON:  $\text{Ce}^{3+}$ ,  $Q = 50000\text{ cm}^{-1}$ ,  $V = 3$ ,  $E_a$  is constant in the same host, the value of E is directly proportional to the product of n and r. The crystal field splitting ( $D_q$ ) can be determined by the following equation<sup>17, 35</sup>:

$$D_q = \frac{1}{6} Z e^2 \frac{r^4}{R^5} \quad (2)$$

where  $D_q$  is a measured energy level separation, Z is the anion charge, e is the electron charge, r is the radius of the d wavefunction, and R is the bond length. As shown in Fig.2 (b), among the four sites, Y1 has the loosest site (CN=8), the largest n value and average bond length (2.492  $\text{\AA}$ ), so according to equ (1) and (2), it corresponding to the smallest E value and weakest crystal field splitting. So Y1 accommodate  $\text{Ce}^{3+}$  activators to correspond with the

highest energy (shortest-wavelength) emission peak (413 nm, 448 nm). While Y3 has the tightest site (CN=6), the smallest  $n$  value and average bond length (2.313 Å), it corresponding to the largest  $E$  value and strongest crystal field splitting. So Y3 accommodate  $Ce^{3+}$  activators to correspond with the lowest energy (longest-wavelength) emission peak (619 nm, 698 nm).

The Y2 and Y4 sites have the same 7 coordination number, and both the average bond length  $R$  and anion charge  $Z$  of Y2 site is smaller than that of Y4 site. Thus the emission bands of Y2 and Y4 sites can't be determined effectively by equ. (1) and (2). However, the emission site is also related to the centroid shift in the  $Ce^{3+}$  ions d-orbitals. The 5d centroid shift for  $Ce^{3+}$  can be expressed by the following equation<sup>36,37</sup>:

$$\varepsilon_c = A \sum_{i=1}^N \frac{a_{SP}^i}{(R_i - 0.6\Delta R)^6} \quad (3)$$

where  $A$  is a constant,  $a_{SP}^i$  is the spectroscopic polarizability of anion  $i$ ,  $R_i$  is the distance between  $Ce^{3+}$  and anion  $i$  in the undistorted lattice, and  $\Delta R$  is the difference between the radii of  $Ce^{3+}$  and  $Y^{3+}$  in different sites. Y2 and Y4 sites have same coordinate number (CN=7), which lead to the same  $Y^{3+}$  ions radius. So  $A$  and  $\Delta R$  are constant,  $a_{SP}^i$  and  $R_i$  are variable. The polarizability  $a_{SP}^i$  of N ligand is larger than that of O ligand due to the smaller electronegativity of N (3.04). The  $R_i$  of Ce-N is slightly larger than Ce-O.<sup>38</sup> Based on the analysis above, the Y4 site has a larger centroid shift than Y2 site. On the other hand, because the difference of electronegativity between  $Ce^{3+}$  and  $N^{3-}$  is smaller than  $Ce^{3+}$  and  $O^{2-}$ , the covalency of Ce-N is stronger than that of Ce-O, which causes the larger nephelauxetic effect. Therefore Y2 site have a shorter emission (428 nm, 469 nm) while Y4 site have a longer emission (512 nm, 569 nm).

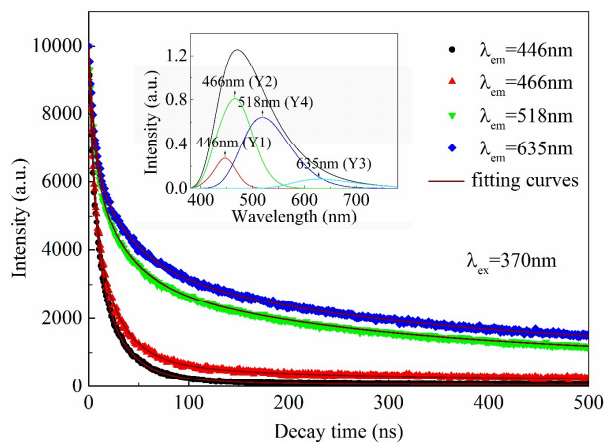


**Fig. 8** PL decay curves of YSAON: 0.01Ce<sup>3+</sup> ( $\lambda_{ex}$ =370 nm;  $\lambda_{em}$ =446 nm,  $\lambda_{em}$ =466 nm,  $\lambda_{em}$ =518 nm and  $\lambda_{em}$ =635 nm).

In order to further confirm that the four emission bands are assigned to Y1, Y2, Y3 and Y4 sites respectively. The PL decay curves of the  $Ce^{3+}$  ions in  $Y_4SiAlO_8N$ : 0.01Ce<sup>3+</sup> phosphors were obtained with an excitation at 370 nm, and monitored at 446 nm, 466 nm, 518 nm and 635 nm (see the inset of Fig. 8), as shown in Fig. 8. It can be seen that the varying decay curves of the  $Ce^{3+}$  ions upon 370 nm excitation can be fitted well to a typical four exponential decay curve using the following equation<sup>17,20</sup>:

$$I(t) = A_1 \exp\left(\frac{-t}{\tau_1}\right) + A_2 \exp\left(\frac{-t}{\tau_2}\right) + A_3 \exp\left(\frac{-t}{\tau_3}\right) + A_4 \exp\left(\frac{-t}{\tau_4}\right) \quad (4)$$

where  $I(t)$  represents the luminescence intensity at time  $t$ ,  $A_1$ ,  $A_2$ ,  $A_3$  and  $A_4$  are constants, and  $\tau_1$ ,  $\tau_2$ ,  $\tau_3$ , and  $\tau_4$  are the four exponential components of the decay time,  $t$  is the time. Using these parameters, the average decay time ( $\tau_{avg}$ ) can be determined by the following formula<sup>17,20</sup>:

$$\tau_{avg} = \frac{A_1\tau_1^2 + A_2\tau_2^2 + A_3\tau_3^2 + A_4\tau_4^2}{A_1\tau_1 + A_2\tau_2 + A_3\tau_3 + A_4\tau_4} \quad (5)$$

Table 3 presents the values of  $A_1$ ,  $A_2$ ,  $A_3$ ,  $A_4$ ,  $\tau_1$ ,  $\tau_2$ ,  $\tau_3$ ,  $\tau_4$  and degree of fitting. Under different monitored wavelength, all the degree of fitting is close to 1, which suggest that the varying decay curves of the  $Ce^{3+}$  ions in YSAON host are suitable for four exponential curve fitting. The average lifetime of the  $Ce^{3+}$  ions are determined to be 121.12ns, 271.21ns, 478.43ns and 525.46ns for YSAON: 0.01Ce<sup>3+</sup> with the monitored wavelength at 446 nm, 466 nm, 518 nm and 635 nm, respectively. In general, the active ions occupied the same site have similar emission decay times.<sup>39</sup> Fig. 8 and Table 3 indicate that the lifetime of  $Ce^{3+}$  in four sites above are different, which can demonstrate the existence of four emission sites in YSAON: 0.01Ce<sup>3+</sup>.

**Table 3.** Measured values of  $A_1$ ,  $A_2$ ,  $A_3$ ,  $A_4$ ,  $\tau_1$ ,  $\tau_2$ ,  $\tau_3$ ,  $\tau_4$  and degree of fitting.

Emission peaks	$A_1$	$A_2$	$A_3$	$A_4$	$\tau_1$ (ns)	$\tau_2$ (ns)	$\tau_3$ (ns)	$\tau_4$ (ns)	$\tau_{avg}$ (ns)	CHISQ
446nm	4300	4200	1500	100	4.6	17.5	43.5	452.4	121.12	1.0466
466nm	4800	4400	600	200	5.3	24.2	94.7	619.2	271.21	0.991
518nm	3700	3300	1600	1400	5.6	30.4	150.8	630.1	478.43	1.047
635nm	3600	2900	1800	1800	6.1	36.6	173.3	669.2	525.46	0.996

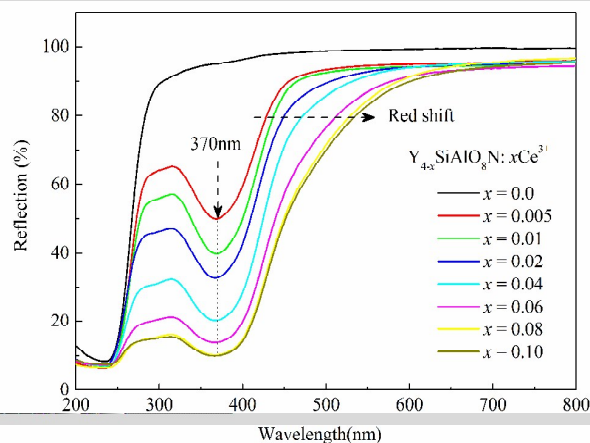


**Fig. 9** Diffuse reflection spectra of doped and undoped YSAON:  $xCe^{3+}$  ( $0 \leq x \leq 0.1$ ).

Fig. 9 shows the diffuse reflection spectra of doped and undoped YSAON:  $xCe^{3+}$  ( $0 \leq x \leq 0.1$ ). As shown in Fig. 9, compared with undoped YSAON host materials, a broad strong absorption band is observed from 250 nm to 500 nm in YSAON:  $xCe^{3+}$  ( $0.005 \leq x \leq 0.1$ ), which is attributed to the  $5d^1 \rightarrow 4f^1$  transition of  $Ce^{3+}$  and is consistent with the PLE spectra. With the increase of  $Ce^{3+}$

concentration, the absorption band appears an obvious red shift. This is because a higher  $\text{Ce}^{3+}$  concentration leads to a compact energy band structure and a smaller band gap, which causes a smaller transition energy  $E$ . According to  $E=hc/\lambda$ , hence a higher  $\text{Ce}^{3+}$  concentration can cause a red shift.

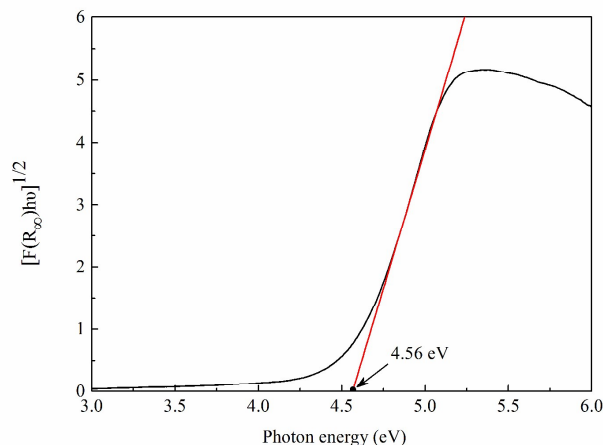


**Fig. 10** Absorption spectra of YSAON host as calculated by the Kubelka-Munk formula.

The band gap of the YSAON host can be estimated according to eqn (6)<sup>40</sup>:

$$[F(R_{\infty})hv]^n = A(hv - E_g) \quad (6)$$

where  $hv$  is the photon energy,  $A$  is a proportional constant,  $E_g$  is the value of the band gap,  $n = 2$  for a direct transition or  $1/2$  for an indirect transition, and  $F(R_{\infty})$  is the Kubelka-Munk function, with  $F(R_{\infty}) = (1-R)^2/2R$ , and  $R$  is the observed reflectance in the Fig. 9.

The values of  $[F(R_{\infty})hv]^n$  are plotted as a function of the incident photon energy ( $hv$ ) as illustrated in the Figure 10. From the linear extrapolation of  $[F(R_{\infty})hv]^n = 0$ , the  $E_g$  value was estimated to be about 4.56 eV, which is slightly larger than the value of 3.819 eV obtained from DFT calculation. This is because the energy states of samples were geometry optimized before DFT calculation in order to obtain the most stable structure and lowest energy states.

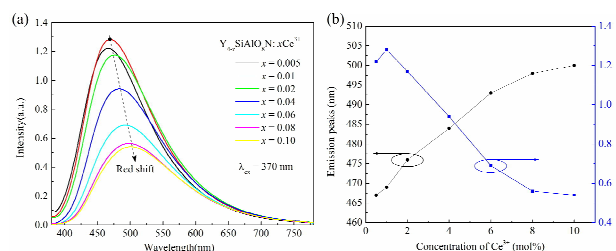


**Fig. 11** (a) PL spectra of YSAON:  $x\text{Ce}^{3+}$  ( $x = 0.005, 0.01, 0.02, 0.04, 0.06, 0.08$  and  $0.10$ ). (b) The linear relation of the emission peaks and relative intensity with the increase of  $\text{Ce}^{3+}$  concentration.

The influence of the  $\text{Ce}^{3+}$  concentration on the luminescence properties is presented in Fig. 11. With increasing  $\text{Ce}^{3+}$  concentration, the luminescence intensity increases and then decrease, reaches a maximum at  $x = 0.01$ . It is mainly attributed to the energy transfer among  $\text{Ce}^{3+}$  ions, which may occur via exchange

interaction, radiation reabsorption, or multipole-multipole interaction. With increasing amount of doped  $\text{Ce}^{3+}$ , the distance between  $\text{Ce}^{3+}$  ions shortens, which increases the probability of non-radiative energy transfer between  $\text{Ce}^{3+}$  ions. The critical distance for energy transfer can be roughly calculated using eqn (7)<sup>16,22</sup>,

$$R_c = 2 \left( \frac{3V}{4\pi x_c N} \right)^{1/3} \quad (7)$$

Where  $x_c$  is the critical concentration,  $N$  is the number of cation sites in the unit cell, and  $V$  is the volume of the unit cell. In this case,  $V = 805.83 \text{ \AA}^3$ ,  $N = 16$  and the critical doping concentration of  $\text{Ce}^{3+}$  in YSAON host is found to be 0.01. According to the above equation,  $R_c$  of  $\text{Ce}^{3+}$  was then determined to be 21.27  $\text{\AA}$ . Thus, it can be inferred that the mechanism of exchange interaction plays no role in energy transfer between  $\text{Ce}^{3+}$  ions in YSAON host since the exchange interaction requires a forbidden transition and a typical critical distance less than 5  $\text{\AA}$ .<sup>41, 42</sup> Therefore, according to the Dexter theory, the non-radiative transitions between  $\text{Ce}^{3+}$  ions happened via electric multipolar interactions.<sup>42</sup>

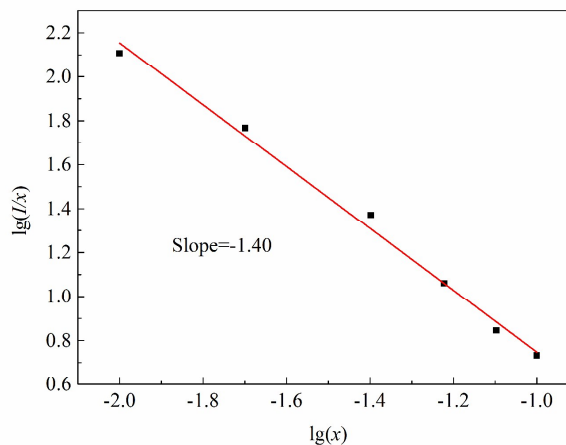


**Fig. 12** The relationships of  $\lg(x)$  versus  $\lg(I/x)$ .

The interaction type between sensitizers or and activator can be calculated by the following equation (8)<sup>42,43</sup>:

$$I/x = k \left[ 1 + \beta(x)^{\theta/3} \right]^{-1} \quad (8)$$

Here,  $x$  is the activator concentration,  $I/x$  is the emission intensity ( $I$ ) per activator concentration ( $x$ ),  $k$  and  $\beta$  are constants for the same excitation condition, and  $\theta$  is a function of multipole-multipole interaction. When the value of  $\theta$  is 6, 8 or 10, the form of the interaction corresponds to dipole-dipole (d-d), dipole-quadrupole (d-q), or quadrupole-quadrupole (q-q) respectively. To determine the  $\theta$  value, the relationship between  $\lg(I/x)$  and  $\lg(x)$  is plotted in Fig. 12. The slope of the straight line is  $-1.4$  which equals  $-\theta/3$ . Thus, the value of  $\theta$  is calculated to be 4.2, which is mostly close to 6, suggesting that the quenching in YSAON:  $x\text{Ce}^{3+}$  phosphors most likely results from dipole-dipole interactions. Besides, as shown in Fig. 6(a), there are small overlap between the excitation and emission spectra in the range from 400 nm to 450 nm. Thus, the contribution of reabsorption plays another role in causing concentration quenching.

### 3.5 Emission spectra and CIE chromaticity coordinates of $Y_4SiAlO_8N: 0.01Ce^{3+}, ySm^{3+}$

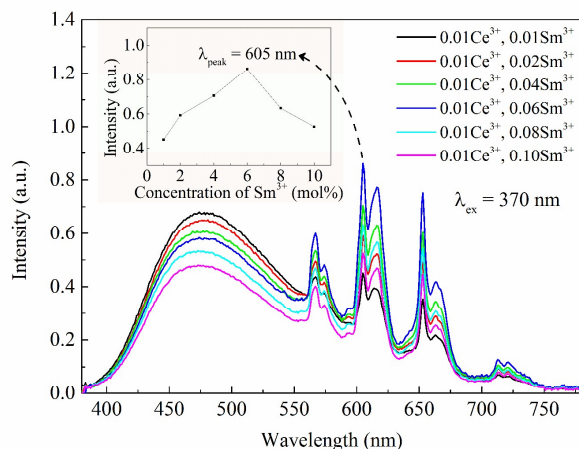


Fig. 13 PLE and PL spectra of  $Y_4SiAlO_8N: 0.01Ce^{3+}, ySm^{3+}$  phosphors.

Fig. 13 indicates the emission spectra of the  $Y_4SiAlO_8N: 0.01Ce^{3+}, ySm^{3+}$  ( $0.01 \leq y \leq 0.1$ ) phosphors under 370 nm excitation. All the emission spectra are composed of a splitting blue band ( $Ce^{3+}$  emission) and three reddish-orange bands ( $Sm^{3+}$  emission). In the  $YSAON: 0.01Ce^{3+}, ySm^{3+}$  samples, the emission intensity of  $Ce^{3+}$  decrease monotonically and that of  $Sm^{3+}$  increase firstly and then decrease (reach a maximum at  $y = 0.06$ ) with increasing  $Sm^{3+}$  concentration. The change of emission intensity of  $Sm^{3+}$  attributed to the results of  $Sm^{3+}$ - $Sm^{3+}$  concentration quenching and interaction between  $Ce^{3+}$  and  $Sm^{3+}$ . The decrease of emission intensity of  $Ce^{3+}$  can be ascribed to the competitive absorption between  $Ce^{3+}$  and  $Sm^{3+}$ , which could be verified by the Fig. 6.

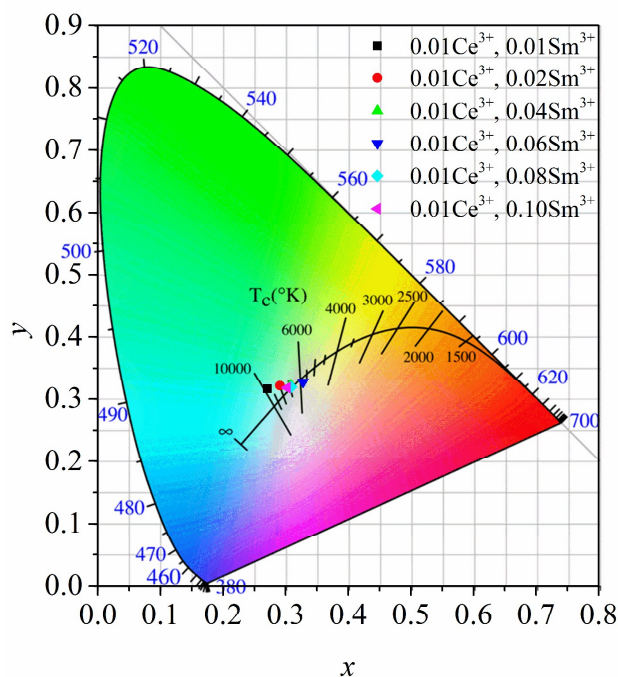


Fig. 14 CIE chromaticity diagram for  $YSAON: 0.01Ce^{3+}, ySm^{3+}$  phosphors with different doping concentrations of  $Sm^{3+}$  ions.

The CIE chromaticity coordinates of  $YSAON: 0.01Ce^{3+}, ySm^{3+}$  phosphors with different  $Sm^{3+}$  dopant contents are shown in Fig. 14. The measured chromaticity coordinates ( $X, Y$ ) for  $YSAON: 0.01Ce^{3+}, ySm^{3+}$  phosphors are listed in Table 4. As shown in Fig. 14, by control the concentration of doped  $Sm^{3+}$ , the chromaticity coordinates ( $X, Y$ )  $YSAON: 0.01Ce^{3+}, ySm^{3+}$  ( $y=0.04, 0.06, 0.08$  and  $0.10$ ) can pass through the Planckian black-body radiator that radiates light of comparable hue to that white light source.

Table 4. Measured values of  $A_1, A_2, A_3, A_4, \tau_1, \tau_2, \tau_3, \tau_4$  and degree of fitting.

Different $y$ values	CIE coordinates		CCTs(K)
	$x$	$y$	
$y=0.01$	0.2709	0.3165	9587
$y=0.02$	0.2909	0.3215	7940
$y=0.04$	0.308	0.3229	6824
$y=0.06$	0.3277	0.3274	5718
$y=0.08$	0.3089	0.3194	6802
$y=0.10$	0.3027	0.318	7210

Moreover, for phosphors, correlated color temperature (CCT) is another important parameter, which is calculated using the following approximate formula reported by McCamy:  $T = -437n^3 + 3601n^2 - 6861n + 5514.31$ , where  $n = (x - 0.3320)/(y - 0.1858)$ . The calculated and measured results listed in Table 3, which indicate that  $YSAON: 0.01Ce^{3+}, ySm^{3+}$  emit cool white light. When the value of  $y$  increases to 0.06, the smallest CCT value of 5718 K can be obtained, which is consistent with the highest emission intensity of  $Sm^{3+}$ . These results indicate that the white light can successfully be obtained by co-doping  $Ce^{3+}$  and  $Sm^{3+}$  ions into  $Y_4SiAlO_8N$  host lattice, which is suitable for use in 370 nm near-UV light chips.

## 4 Conclusions

In summary,  $Y_4SiAlO_8N: Ce^{3+}, Sm^{3+}$  phosphors are successfully synthesized by a conventional solid-state reaction method. The XRD refinement results indicate that pure  $Y_4SiAlO_8N$  phase has been obtained. The crystal structure of  $Y_4SiAlO_8N$  was solved and refined as monoclinic system and space group  $P121/c1$  (14) with  $a=7.4491\text{\AA}$ ,  $b=10.3933\text{\AA}$ ,  $c=11.0563\text{\AA}$ ,  $\beta=109.7109^\circ$ . The DFT calculation indicates that  $Y_4SiAlO_8N$  has an indirect band gap of 3.819 eV that can provide an appropriate environment for the  $Ce^{3+}$  and  $Sm^{3+}$  emission. The four emission sites of  $Y_4SiAlO_8N: 0.02Ce^{3+}$  is determined as Y1 (413 nm, 448 nm), Y2 (428 nm, 469 nm), Y3 (619 nm, 698 nm) and Y4 (512 nm, 569 nm), respectively. The diffuse reflection spectra show that  $Y_4SiAlO_8N: Ce^{3+}$  has a board absorption band that in the range of 250-500 nm, which are consistent with the PLE spectra. The PLE and PL spectra measurements showed that the  $Ce^{3+}$  and  $Sm^{3+}$  co-doped phosphor could be efficiently excited by near-UV light, and exhibited four emission bands peaked at 485 nm, 565 nm, 605 nm and 650 nm respectively. The concentration quenching mechanism of  $Ce^{3+}$  in  $Y_4SiAlO_8N$  is discussed in detail and is confirmed as dipole-dipole interactions. The CIE chromaticity of obtained white light can pass through by adjusting the content of  $Ce^{3+}$  and  $Sm^{3+}$  ions. Therefore,

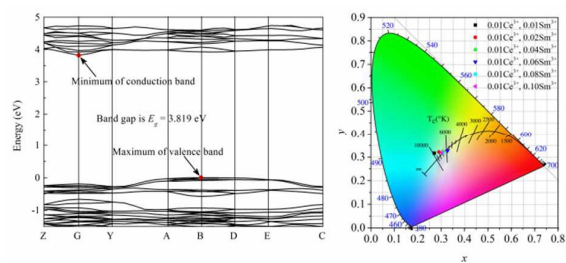
we anticipate that these materials can be used in near-UV chip pumped white LEDs.

## Acknowledgements

This work was financially supported by the National Natural Science Foundation of China (Grant nos. 51272243 and 61405185), the Zhejiang Provincial Natural Science Foundation of China (LY14E020008 and LZ14F050001).

## Notes and references

- J. Y. Tsao, M. H. Crawford, M. E. Coltrin, A. J. Fischer, D. D. Koleske, G. S. Subramania, G. T. Wang, J. J. Wierer, and R. F. Karlicek Jr., *Adv. Optical Mater.*, 2014, **2**, 809–836.
- P. Pust, P. J. Schmidt and W. Schnick, *Nat. Mater.*, 2015, **14**, 454–458.
- S. Nakamura and G. Fasol, *The Blue Laser Diode: GaN-Based Light Emitting Diode and Lasers*, Springer, Berlin, 1997.
- H.-S. Roh, D. H. Kim, I.-J. Park, H. J. Song, S. Hur, D.-W. Kim and K. S. Hong, *J. Mater. Chem.*, 2012, **22**, 12275–12280.
- R. Kasuya and T. Isobe, *J. Phys. Chem. B*, 2005, **109**, 22126–22130.
- G. Gu, W. Xiang, C. Yang and X. Liang, *CrystEngComm*, 2015, **17**, 4554–4561.
- J. S. Cho, K. Y. Jung and Y. C. Kang, *RSC Adv.*, 2015, **5**, 8345–8350.
- J. K. Sheu, S. J. Chang, C. H. Kuo, Y. K. Su, Senior Member, IEEE, L. W. Wu, Y. C. Lin, W. C. Lai, J. M. Tsai, G. C. Chi, and R. K. Wu, *Photonics Technology Letters, IEEE*, 2003, **15**(1), 18–20.
- J. W. Li, T. Watanabe, N. Sakamoto, H. S. Wada, T. Setoyama and M. Yoshimura, *Chem. Mater.*, 2008, **20**, 2095.
- Y. Kim, J. Kim and S. Kang, *J. Mater. Chem. C*, 2013, **1**, 69–78.
- K. J. D. MacKenzie, G. J. Gainsford and M. J. Ryan, *J. Eur. Ceram. Soc.*, 1996, **16**, 553–560.
- M. J. Pomeroy and S. Hampshire, *J. Ceram. Soc. Jpn.*, 2008, **116**, 722–726.
- J. W. H. Krevel, H.T. Hintzen, R. Metselaar and A. Meijerink, *J. Alloy. Compd.*, 1998, **268**, 272–277.
- F. C. Lu, X. Y. Chen, M. W. Wang and Q. L. Liu, *J. Lumin.*, 2011, **131**, 336–341.
- F.C. Lu, X.P. Song and Q.L. Liu, *Opt. Mater.*, 2010, **33**, 91–98.
- Z. Xia and W. Wu, *Dalton Trans.*, 2013, **42**, 12989–12997.
- Q. Wu, Z. Yang, Z. Zhao, M. Que, X. Wang and Y. Wang, *J. Mater. Chem. C*, 2014, **2**, 4967–4973.
- F.C. Lu, S. Guo, Z. Yang, Y. Yang, P. Li, X. Li and Q. Liu, *J. Alloy. Compd.*, 2012, **521**, 77–82.
- D. Deng, S. Xu, X. Su, Q. Wang, Y. Li, G. Li, Y. Hua and L. Huang, *Mater. Lett.*, 2011, **65**, 1176–1178.
- D. Geng, H. Lian, M. Shang, Y. Zhang and J. Lin, *Inorg. Chem.*, 2014, **53**, 2230–2239.
- K. Liddell, H. Mandal and D. P. Thompson, *J. Eur. Ceram. Soc.*, 1997, **17**, 781–787.
- W. Liu, C. Yeh, C. Huang, C. Lin, Y. Chiu, Y. Yeh and R.-S. Liu, *J. Mater. Chem.*, 2011, **21**, 3740–3744.
- W. B. Park, S. P. Singh, M. Pyo and K. S. Sohn, *J. Mater. Chem.*, 2011, **21**, 5780–5785.
- R. M. Martin, *Electronic Structure*, Cambridge University Press, Cambridge, 2004.
- J. Tang, J. Gao, J. Chen, L. Hao, X. Xu and M.-H. Lee, *Comput. Mater. Sci.*, 2013, **79**, 478.
- T. M. Tolhurst, T. D. Boyko, P. Pust, N. W. Johnson, W. Schnick and A. Moewes, *Adv. Optical Mater.*, 2015, **3**, 546–550.
- Z. Xia, C. Ma, M. S. Molokeev, Q. Liu, K. Rickert and K. R. Poeppelmeier, *J. Am. Chem. Soc.*, 2015, **137**, 12494–12497.
- Z. Xia, M. S. Molokeev, W. B. Im, S. Unithrattil, Q. Liu, *J. Phys. Chem. C*, 2015, **119**, 9488–9495.
- X. M. Wang, C. H. Wang, X. J. Kuang, R. Q. Zou, Y. X. Wang and X. P. Jing, *Inorg. Chem.*, 2012, **51**, 3540–3547.
- Z. Cui, R. Ye, D. Deng, Y. Hua, S. Zhao, G. Jia, C. Li and S. Xu, *J. Alloy. Compd.*, 2011, **509**, 3553–3558.
- H. Yang and Y. Kim, *J. Lumin.*, 2008, **128**, 1570–1576.
- L. Seijo and Z. Barandiaran, *Phys. Chem. Chem. Phys.*, 2013, **15**, 19221.
- G. Blasse and A. Bril, *J. Chem. Phys.*, 1967, **47**, 5139.
- L. V. Uitert and *J. Lumin.*, 1984, **29**, 1–9.
- P. D. Rack and P. H. Holloway, *Mater. Sci. Eng.*, 1998, **21**, 171.
- S. Miao, Z. Xia, M. S. Molokeev, M. Chen, J. Zhang, Q. Liu, *J. Mater. Chem. C*, 2015, **3**, 4616.
- X. Li, Y. Hua, H. Ma, D. Deng and S. Xu, *CrystEngComm*, 2015, **17**, 9123.
- Shannon, R. D., *Acta Cryst.*, 1976, **A32**, 751.
- Y. Chen, Y. Li, J. Wang, M. Wu, and C. Wang, *J. Phys. Chem. C*, 2014, **118**, 12494–12499.
- D. Deng, H. Yu, Y. Li, Y. Hua, G. Jia, S. Zhao, H. Wang, L. Huang, Y. Li, C. Li and S. Xu, *J. Mater. Chem. C*, 2013, **1**, 3194.
- Z. Xia, R. S. Liu, K. W. Huang and V. Drozd, *J. Mater. Chem.*, 2012, **22**, 15183–15189.
- D. L. Dexter, *J. Chem. Phys.*, 1953, **21**, 836.
- G. Blasse, *Phys. Lett. A*, 1968, **28**, 444.
- C. S. McCamy, *Color Res. Appl.*, 1992, **17**, 142–144.



The band structure and CIE chromaticity coordinates of  $\text{Y}_4\text{SiAlO}_8\text{N}: 0.01\text{Ce}^{3+}, y\text{Sm}^{3+}$  phosphors were studied.